LANGMUIR

Article

pubs.acs.org/Langmuir

Diverse Bilayer Morphologies Achieved via α-Helix-to-β-Sheet Transitions in a Short Amphiphilic Peptide

H. Christopher Fry,*[,†] Gleiciani de Q. Silveira,[†] Hannah M. Cohn,[†,§] and Byeongdu Lee[‡]

[†]Center for Nanoscale Materials and [‡]Advanced Photon Source, Argonne National Laboratory, Argonne, Illinois 60439, United States

Supporting Information

ABSTRACT: Transmembrane proteins are functional macromolecules that direct the flow of small molecules and ions across a lipid bilayer. Here, we propose the development of helical peptide amphiphiles that will serve as both the bilayer and the functional unit of a self-assembled peptide bilayer membrane. The peptide, K_3L_{12}, was designed not only to possess dimensions similar to that of a lipid bilayer but also to yield a structurally robust, α-helical bilayer. The formation of α-helices is pH-dependent, and upon annealing the sample, a transition from α-helices to β-sheets can be controlled, as indicated by optical and vibrational spectroscopies. Imaging the materials confirms morphologies similar to that of a lipid bilayer but rich in α-helices. Annealing the samples yields a shift in the morphology from bilayers to curled disks, fibers, and sheets. The structural robustness of the material can facilitate the incorporation of many functions into the bilayer assembly.

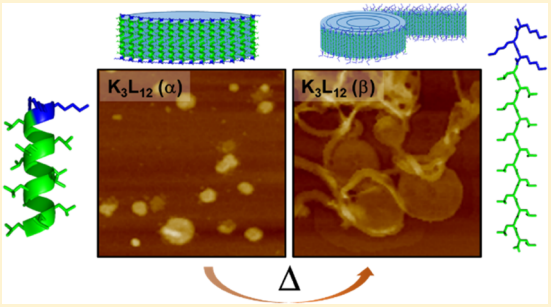

INTRODUCTION

The lipid bilayer represents the medium in which transmembrane proteins are housed and execute their diverse array of functions such as transferring electrons, ions, and molecules across the membrane that subsequently signals a cascade of events including catalysis.[1,2] At a very basic level, the bilayer and the transmembrane protein combine to form the functional material. To generate a functional membrane that applies both the amphiphilic nature of the lipid and the structural requirements of a protein, the careful design of short peptides is considered.[3,4] We suggest that the first step when generating a functional peptide bilayer is demonstrating control over the secondary structure of the assembly. Here, we present a small (15 mer) peptide that not only assembles into dimensions similar to that of the lipid bilayer (∼4 nm) but also possesses a high degree of α-helical content. Upon heating, these α-helical structures can transition into β-sheet-rich assemblies and adopt unique morphologies.

Self-assembling peptide materials demonstrate a diverse array of functional materials.[5−7] They are often deemed functional via the incorporation of a biorecognition epitope for targeting specific cell receptors.[8] However, this renders the peptide assembly as structural support with little function. Nature, on the other hand, employs proteins to carry out innumerable functions. Function is achieved via the precise folding of the protein where specific amino acids are placed proximal to one another. Recent advances in peptide materials have demonstrated this spatial precision such that functional motifs like catalytic triads and cofactor binding sites (e.g., ions, transition metals, small signaling molecules, chromophores) have been realized.[9] Too often, reports of peptide materials ignore the importance of the secondary structure. Peptide amphiphiles are overrun with β-sheet-rich, long-aspect-ratio nanofibers.[7] Collagen or collagen-inspired assemblies and other coiled-coil assemblies dominate reports of α-helix-rich materials where the helix axis lies along the axis of the resulting fiber.[10−12] KL minimalist peptides have a rich history and they tend to focus on repeat units (e.g., $(KL)_n$, $(KLL)_n$, $(KLLL)_n$, $(LKKL)_n$, etc.) instead of diblock structures.[13] Due to their highly cationic nature, they are typically investigated as antimicrobial reagents.[14] Circular dichroism spectroscopy of these peptides suggests structurally complex folding but the link between spectroscopy and morphology was not investigated. In larger polypeptides, K_nL_m diblock copolymers, where $n > 20$ and $m > 10$, the ratio of K to L was varied to explore the control over morphology (e.g., sheets vs vesicles and vesicle size).[15,16] More recently, a molecular dynamics investigation explored the parallel vs antiparallel orientation of a monolayer of α-helix-rich $K_{10}L_{10}$.[17] While it was found that both parallel and antiparallel models yielded stable monolayers, future work was proposed to investigate bilayers of α-helical diblock peptides.

The peptide $H_2N{-}K_3L_{12}{-}CONH_2$ (referred to simply as K_3L_{12}) was chosen because the dimensions of the designed peptide assemblies are reminiscent of a lipid bilayer, a 3.6 nm hydrophobic region, and a short-charged region (Figure 1). The N-terminus was intentionally left unmodified (H_2N-) as it resides in the charged end of the amphiphilic molecule. A

Received: February 11, 2019
Revised: May 6, 2019
Published: June 13, 2019

DOI: 10.1021/acs.langmuir.9b00424
Langmuir XXXX, XXX, XXX−XXX

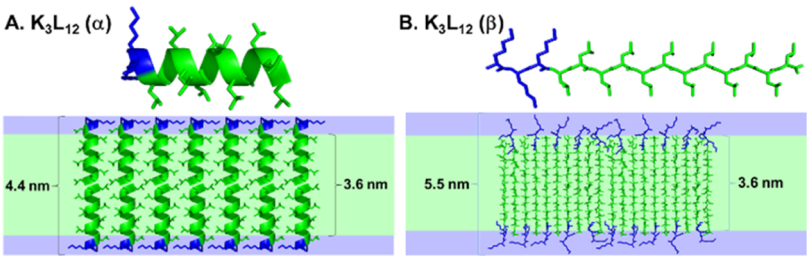

Figure 1. K_3L_{12} depicted as an A. α-helix and B. β-sheet monomer. Their respective bilayer assemblies highlight the similar dimensions to that of a lipid bilayer. Lysine is depicted in blue and leucine in green.

neutral carboxamide (-$CONH_2$) C-terminus was employed to prevent charge in the proposed hydrophobic interior of the assembly. Although leucine often demonstrates proficiency for α-helix formation, data pertaining to amino acid propensity favoring α-helices versus β-sheets suggest that leucine is found equally in both conformations and have been modeled (Figure 1).[18] In addition, leucine was specifically chosen due to the well-documented leucine zipper motif in the peptide helix design.[19] The leucine-rich helical region facilitates helix−helix packing between neighboring molecules, thus stabilizing the material via noncovalent interactions. Furthermore, according to experimentally determined hydrophobicity scales,[20,21] positively charged lysine is exceedingly more hydrophilic than the neutral, leucine. As such, we propose that upon dissolution in aqueous solutions, the charged lysine head group of K_3L_{12} is preferably on the exterior of the assembly where it is exposed to water. The hydrophobic leucine block at the neutral carboxamide C-terminus will bury itself as it will exclude or minimize water content from the interior of the resulting assemblies. Here, we present that K_3L_{12} yields α-helix-rich bilayer assemblies that are morphologically dependent on pH. Furthermore, annealing the samples promotes a secondary structural transition from α-helices to β-sheets that concurrently transitions the morphology of the material from disks to rolled tapes at low pH. At high pH, α-helix-rich spheres transition to α-helix-rich planks. These structural transitions induced by pH and temperature highlight the importance of considering secondary structure when designing peptides as functional materials.

MATERIALS AND METHODS

The peptide assembly was designed with the assistance of Hyperchem 8.0. Idealized α-helices and parallel β-sheet ϕ/Ψ angles were used to determine the dimensions of the folded peptide; $H_2N-K_3L_{12}-CONH_2$ CHARMM force fields were used for energy minimization studies (in vacuo) to provide a better understanding of intermolecular distances.

The peptide was synthesized using standard Fmoc solid-phase peptide synthesis procedures with reagents and Fmoc-protected amino acids sourced from Chem Impex Inc. and solvents (dimethylformamide, dichloromethane, diisopropylethylamine, piperidine, trifluoroacetic acid, and triisopropylsilane) purchased from Sigma-Aldrich. Briefly, 0.1 mmol of a low-load rink amide MBHA resin (0.39 mmol/g) was successively Fmoc-deprotected with 25% piperidine in dimethylformamide and coupled to 1 mmol Fmoc-Leu-OH (12×) and Fmoc-Lys(Boc)-OH (3×) activated with 1 mmol HBTU to yield the protected $H_2N-K_3L_{12}-CONH_2$. Cleavage from the resin and deprotection were achieved via suspending the resin in 10 mL of 95:2.5:2.5 TFA/TIPS/water solution and stirring slowly for 6 h at RT. The resulting solution was filtered, and the filtrate was added dropwise into 100 mL of cold diethyl ether to precipitate the crude material. Further purification was achieved by RP-HPLC. Crude peptide (2 mg) was dissolved in 20 μL of hexafluoroisopropanol followed by the addition of 1 mL of water/acetonitrile (1:1) and 0.1% of TFA. The sample was purified via a linear gradient on a reverse phase C18 HPLC column (10 × 250 mm Jupiter Proteo, Phenomenex) beginning with 50:50 water/acetonitrile (0.1% TFA) and increasing to 100% acetonitrile over 50 min, where the sample eluted at 84% acetonitrile. The fractions of multiple purification runs were combined and freeze-dried to yield pure K_3L_{12}. Electrospray ionization mass spectrometry was obtained using an Advion expression compact mass spectrometer (CMS).

Circular dichroism was performed with a JASCO-815 spectrophotometer (scanning from 260 to 190 nm) with 100 μM solutions in a 1 mm path length quartz cuvette.

pH Variation. Stock solutions of $H_2N-K_3L_{12}-CONH_2$ were prepared in hexafluoroisopropanol at high concentrations (10 wt %, 53 mM). Typical sample preparation includes dilution via pipette addition of 0.6 μL of stock solution into 10 μL of water in a 1.5 mL Eppendorf tube. Then, 3 × 96 μL of either 100 mM HCl, Millipore water (18.2 MΩ), or 100 mM NH_4OH was added to the solution while vortexing to ensure rapid mixing. The final concentration of the peptide was 100 μM. pH was varied by adjusting the molarity of HCl (from 100 to 500 mM, 10 samples with 50 mM steps in HCl concentration) or NH_4OH (100−500 mM, 10 samples with 50 mM steps in NH_4OH concentration). pH values were measured with a Mettler-Toledo S20 seven easy pH meter coupled to a microelectrode (ORION 9110DJWP).

Temperature Dependence. Sample preparation includes dilution via pipette addition of 0.6 μL of stock solution into 10 μL of water in a 1.5 mL Eppendorf tube. Then, 3 × 96 μL of either 100 mM HCl, Millipore water (18.2 MΩ), or 100 mM NH_4OH was added to the solution while vortexing to ensure rapid mixing. The pH values were recorded with the previously described pH microelectrode. The temperature was increased from 20 to 90 °C with 10 °C steps in a capped 1 mm quartz cuvette to minimize solvent evaporation. After reaching 90 °C, the samples were cooled to 20 °C to emphasize irreversibility after annealing.

Time. The same samples from the temperature dependence studies (100 mM HCl, water, 100 mM NH_4OH) were prepared to investigate the kinetics of secondary structural changes. Spectra were measured once per hour for the first 7 h and then once every 24 h.

Infrared spectroscopy was performed on a Nicolet FTIR by depositing 10 μL droplets of $H_2N-K_3L_{12}-CONH_2$ (100 mM) solutions on a CaF_2 window (Sigma-Aldrich) and allowing the droplet to completely dry. Samples (300 μL) were prepared with 100 mM HCl, 10 mM HCl, 1 mM HCl, water, 0.1 mM NH_4OH, 1 mM NH_4OH, 10 mM NH_4OH, and 100 mM NH_4OH. pH values were recorded with the previously described microelectrode. Drops (10 μL) of the samples were deposited on a CaF_2 window and dried under ambient conditions. In addition, samples were annealed at 80 °C for 30 min in capped Eppendorf tubes (to prevent solvent evaporation) and cooled down to room temperature before depositing 10 mL of drops on a CaF_2 window and drying under ambient conditions.

Solution measurements were made in a liquid cell (two CaF_2 windows separated by a Teflon spacer in a stainless steel mount). We prepared 100 μL samples at 1 mM $H_2N-K_3L_{12}-CONH_2$ concentration (1.9 mL of 10 wt % stock solution added to 98 μL)

DOI: 10.1021/acs.langmuir.9b00424
Langmuir XXXX, XXX, XXX−XXX

in deuterated aqueous solutions: 100 mM DCl, 10 mM DCl, 1 mM DCl, D_2O, 1 mM ND_4OD, 10 mM ND_4OD, 100 mM ND_4OD. Sample (50 μL) was added to the liquid cell. The remaining 50 μL was annealed at 80 °C for 30 min and cooled down to room temperature prior to measurement. Amide I vibrations of samples in D_2O (α-helix = 1653 cm^{-1}, β-sheet = 1624 cm^{-1}) are slightly shifted from the dried, nondeuterated samples (α-helix = 1656 cm^{-1}, β-sheet = 1627 cm^{-1}).[22]

Dynamic light scattering was performed on a Malvern Zetasizer. The same samples that were analyzed by circular dichroism spectroscopy were analyzed by dynamic light scattering: 100 μM samples in (1) 100 mM HCl, (2) water, and (3) 100 mM NH_4OH. To emphasize the assembly at low and high pH and minimal assembly at neutral pH, the samples were filtered with a Teflon syringe filter pore size of 0.22 mm and measured again.

Atomic force microscopy was obtained on a Bruker MultiMode 8 microscope using the Scanasyst mode. A silicon tip on a nitride lever was used (Scanasyst-Air Probe, Bruker). Samples were prepared via drop-casting 10 μL of a 100 μM sample in a pool of 100 μL of water on freshly cleaved mica. After 30 s, the solution was removed via pipette followed by wicking away the remaining solution with filter paper. Images (2 μm × 2 μm) were collected at a scan rate of 1 Hz.

Small-angle X-ray scattering (SAXS) and wide-angle X-ray scattering (WAXS) data were simultaneously collected at the Advanced Photon Source at Argonne National Laboratory at beamline 12-ID-B with detectors Pilatus2M and Pilatus300k, respectively. Solution samples (100 μM samples in (1) 100 mM HCl, (2) water, and (3) 100 mM NH_4OH) in 1.5 mm quartz capillaries were scanned to minimize beam damage and subjected to a 0.1 s exposure time, 0.2 mm intervals, and 20 total shots per sample. The scattering angle was calibrated using silver behenate as a standard. Two-dimensional (2D) images were then converted to 1D curves, and the 20 curves for each sample were then averaged. The water background was measured separately and subtracted from the averaged data.

RESULTS AND DISCUSSION

To afford an assembly that is reminiscent of a lipid bilayer, we targeted an assembly with a hydrophobic region of 3.6 nm. Dimensional analysis of the monomeric peptide, K_3L_{12}, in an α-helical conformation yields a peptide that is 2.2 nm in length. Modeling the peptide as an end-to-end bilayer structure in which the helices are hexagonally packed yields a material that is 4.4 nm high with a 3.6 nm hydrophobic region and helix−helix distances of 1.5 nm (Figure S1). While the end-to-end assembly represents our target structure, other structures cannot be ruled out. If we assume an antiparallel α-helix assembly where the molecules are interdigitated, the height was determined to be 2.6 nm (Figure S2). In the event that the secondary structure transitions to β-sheets, in an antiparallel arrangement, we find the peptide to yield ∼5 nm high assemblies (Figure S3). The β-sheet structure promotes hydrogen-bonding interactions in one direction, ultimately producing long-aspect-ratio nanostructures like ribbons and fibers with an intermolecular distance typical for those found for β-sheets, ∼4.5 Å. In addition, the β-sheet assembly yields a leucine-rich face ideal for hydrophobic packing, where the intermolecular distance between neighboring polypeptide backbones was determined, 11.1 (±0.7) Å (Figure S3).

Solid-phase peptide synthesis and purification via RP-HPLC yielded $H_2N-K_3L_{12}-CONH_2$ as a pure material, and electrospray ionization mass spectroscopy was employed to identify the correct mass (Figure S4). To prepare samples for analysis, we first dissolved the peptide in hexafluoroisopropanol at 10 wt % (w/v) or 53 mM. To analyze the resulting assemblies' dependence on pH, we prepared samples in three different conditions: 100 mM HCl, water, and 100 mM NH_4OH. The samples were first diluted in a minimal amount of water (10 μL) followed by the addition of the solvent (3 × 96 μL) to achieve a 300 μL sample yielding a final K_3L_{12} concentration of 100 μM. The samples' secondary structure and morphology were monitored as a function of both pH and temperature.

From pH 0.7 to 10.5, K_3L_{12} exhibited α-helices in all conditions, as indicated by the minima at 208 and 222 nm (Figure 2). The quantity of helical content can be analyzed by

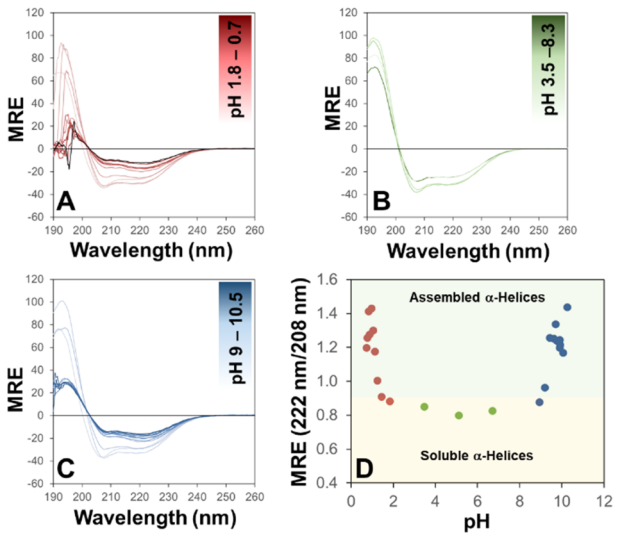

Figure 2. pH Dependence on the secondary structure as determined by CD spectroscopy: K_3L_{12} (100 μM) from (A) pH 0.7 to 1.8 (red), (B) pH 3.5 to 8.3 (green), and (C) pH 9 to 10.5 (blue). (D) Plot of the ratio of the CD signal at 222 and 208 nm (MRE_{222}/MRE_{208}) as a function of pH, soluble helices (yellow region) where MRE_{222}/MRE_{208} < 1, and assembled helices (green region) where MRE_{222}/MRE_{208} > 1.

the mean residue ellipticity.[23] The character of the helices and the extent of the assembly can be interpreted via MRE_{222}/MRE_{208}. When MRE_{222}/MRE_{208} < 1, the α-helices are well solubilized. When MRE_{222}/MRE_{208} > 1, the α-helices are in an environment similar to that found for transmembrane helices. That is, the α-helices are buried in a hydrophobic environment and the sample is most likely scattering light due to the formation of nanoscale assemblies. From pH 2 to 9, MRE_{222}/MRE_{208} = 0.8 (±0.5). When the pH is decreased incrementally, we see the spectrum sharply convert to MRE_{222}/MRE_{208} = 1.30 (±0.10) at pH = 1.0 (300 mM HCl). Interestingly, the same phenomenon occurs at high pH approaching the pK_a of lysine, 10.67 (40 mM NH_4OH), MRE_{222}/MRE_{208} = 1.25 (±0.1), suggesting that the neutralization of the amine decreases the electrostatic repulsion between neighboring molecules allowing higher-order assemblies to form.

While helices are observed immediately upon mixing, assembly into larger structures typically occurs on longer time scales. The samples were aged at room temperature in the dark over a period of 6 days (Figure S5). We were able to probe the stability of the secondary structure with respect to time. Kinetic analysis indicated two major events occurring, a molecular transition in the secondary structure occurred in less than 24 h followed by aggregation over several days. Under neutral conditions, the formation of β-sheets was evident after 1 day of sample aging (τ = 9.8 h). Additional aggregation

DOI: 10.1021/acs.langmuir.9b00424
Langmuir XXXX, XXX, XXX−XXX

occurred over several days where τ = 60 h. At low pH, soluble α-helices transitioned to buried α-helices as evidenced by the evolution of MRE_{222}/MRE_{208} from 0.8 to 1.1 over time, τ = 2 h. Additional assembly was observed with a loss in signal intensity over several days, τ = 48 h. At high pH, the sample was mostly aggregated and rich in helical character upon mixing the sample. The spectrum did not change significantly over 6 days.

Heating the samples incrementally from 10 to 90 °C yielded irreversible transitions at all pH values, Figure 3. At pH values

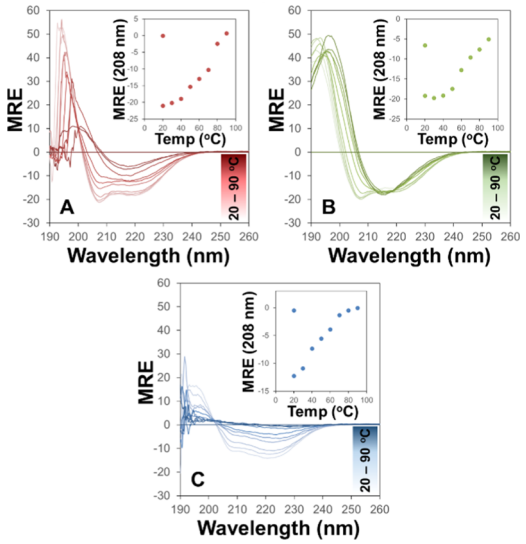

Figure 3. Circular dichroism highlighting temperature dependence on the secondary structure at (A) pH = 1.6 (red), (B) pH = 6.7 (green), and (C) pH 9 (blue). Insets: signal intensity at 208 nm vs temperature.

1.6 and 6.7, we observe the transition from α-helices to β-sheets. The change at low pH is accompanied by a loss in signal intensity, suggesting the formation of higher-order aggregates. At pH > 9, the α-helix is locked into position. Upon heating the sample to 90 °C, the CD spectrum "flattens" due to aggregation.[23] Small- and wide-angle X-ray scattering (Figure S6) revealed the structural transition upon annealing, too. All of the samples at 20 °C at various pH values show broad diffraction peaks at q = 0.565 $Å^{-1}$, indicating that the lateral domain size of the 2D α-helix membrane is small and the interhelix distance is about 1.58 nm ($=2\pi/0.565/\sqrt{3}\times2$) (Figure S1). When they are heated to 80 °C, samples at low pH developed sharp peaks at q = 0.54 $Å^{-1}$ or a d-spacing of 11.5 Å. This peak was particularly strong at pH = 1.5 and is highly consistent with the leucine interface between neighboring fibers, 11.1 (±0.7) Å, Figure S3. The sharp peak breadth indicates that the stacking of the β-sheets is long-range-ordered.

Infrared spectroscopy of both solutions and dried films was measured to monitor the α-helix-to-β-sheet transition (Figures 4 and S7). The dried samples are presented for three reasons: (1) pH-dependent solution IR in D_2O yields a complex amide I spectral region (1550−1750 cm^{-1}) due to interfering H_2O impurities (Figure S7), (2) circular dichroism often can lead to misleading results with nanoscale structures due to scattering (e.g., "flattening"), and (3) amide I vibrations determined in a dried state can be accurately correlated with atomic force microscopy (AFM) sample morphology. Samples (100 μM)

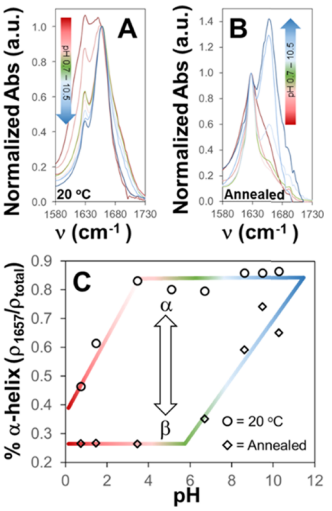

Figure 4. Infrared spectroscopy highlighting the amide I region of K_3L_{12} peptide assemblies dried on CaF_2. (A) At 20 °C, peaks normalized at 1657 cm^{-1} (α-helix) and (B) after heating the sample to 80 °C, peaks normalized at 1627 cm^{-1} (β-sheets). pH changes are represented as acid (red), neutral (green), and basic (blue). (C) Percent of α-helix content at various pH values at 20 °C (open circles) and after heating to 80 °C (open squares).

were first prepared as solutions with a known pH (see SI for details). A small drop of the sample (10 μL) was deposited onto a CaF_2 plate and dried. To analyze the α-helix content, we measured the amide I vibrations and measured the relative area under the peaks corresponding to α-helices (ν = 1657 cm^{-1}) and β-sheets (ν = 1627 cm^{-1}) (Figures 4 and S8). We investigated a range of pH values consistent with that performed in solution and found that under acidic conditions (pH < 2) that β-sheets partially formed upon drying. In the pH range of 3−10.5, we observed that greater than 80% of the dried sample comprised α-helices. After annealing the samples to 80 °C and cooling the sample back to room temperature prior to depositing on a CaF_2 plate, the dried samples from solutions of pH 1−7 were found to be predominately β-sheet (>70%). However, the amount of helical content increased at pH > 8 (~60%). In comparison to the CD data in solution, the transition at neutral conditions is consistent with that of dried films, where a highly α-helical peptide transitions to a β-sheet-rich peptide assembly. However, at low pH, where CD determined that α-helix-rich assemblies began to form, dried samples indicate a high percentage of β-sheets (~50%). After heating the low-pH sample, the CD and IR data are consistent, suggesting a dominant β-sheet structure. At high pH, dried samples indicate high helical content, consistent with CD spectroscopy of solutions. Upon heating this sample, the CD provides uninterpretable results due to spectral "flattening".[23] IR, on the other hand, suggests that the resulting aggregate is composed mostly of α-helices. Overall, temperature and pH provide useful handles when controlling the α-helix-to-β-sheet transition.

These transitions have been well known in the literature,[24−27] but their relationship to nanoscale assemblies of amphiphilic peptides is less explored. Dynamic light scattering of freshly prepared samples was measured. Under neutral conditions, the formation of small aggregate structures (Figure S9). The samples can be filtered and their scattering properties reproduced, suggesting small aggregate sizes. Upon either

DOI: 10.1021/acs.langmuir.9b00424
Langmuir XXXX, XXX, XXX−XXX

increasing or decreasing the pH, we observe larger materials scattering light consistent with the room-temperature CD data, highlighting α-helices consistent with nanoscale assemblies (vide supra). Distribution of the species in solution suggests that the smallest aggregate is ~100 nm. The assemblies are removed via filtration (>0.22 μm, the pore size of the filter) at low- and high-pH solutions. The scattering signal of the filtrate dramatically decreases, suggesting that the removed assemblies are large.

To characterize the morphological transitions between α-helix and β-sheet-rich assemblies, we employ atomic force microscopy. We observed the morphologies (1) immediately after mixing, (2) after 3 days of aging, and (3) after annealing at 80 °C (Figure 5). At low pH, small aggregates change into

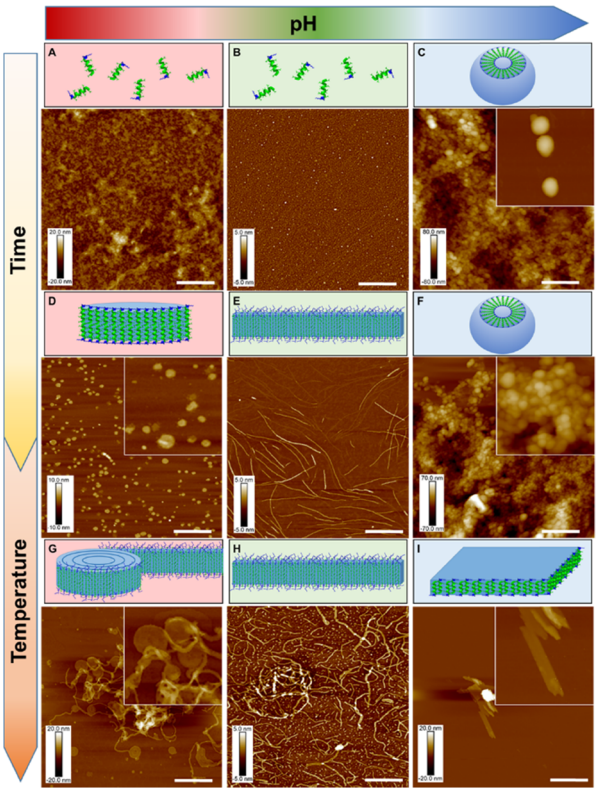

Figure 5. Atomic force micrographs of drop-cast solutions and representative illustrations of K_3L_{12} at 20 °C immediately after preparation at pH (A) 1.6, (B) 6.7, and (C) 9, aged for 3 days at pH D. 1.6, (E) 6.7, and (F) 9, and after annealing at 80 °C at pH (G) 1.6, (H) 6.7, and (I) 9. Scale bar = 400 nm. The insets represent 400 nm × 400 nm details of the images. For height profiles, see Figure S9.

small disks with a 5 nm height (Figures 5A,D and S10) consistent with an end-to-end, bilayer assembly (Figures 1 and S1). After heating the sample, we observe the formation of larger disks (h = 4.6 nm, Figure S10) with fibers "peeling" off the edges (Figure 5G). At neutral conditions, no discernible assembly is observed upon initial drop-casting (Figure 5B), whereas aging and heating the sample yield fibers (Figure 5E,H). Interestingly, the fibers appear to have a ribbonlike dimension (h = 2−4 nm, Figure S10) similar to that of the samples at low pH, but they do not coil into larger-disk assemblies. Finally, at high pH, we observe spheres (Figures 5C and S8). While aging the sample for 3 days does little to change the spheres (Figure 5F), heating completely transitions the spherical aggregates into dense aggregates that possess 3 nm high, planklike structures extending from the edges, Figures 5I and S10. We attribute the shorter height to antiparallel-arranged α-helices (Figure S2) consistent with the IR data (Figure 4).

CONCLUSIONS

The generation of self-assembled peptide amphiphilic materials is well documented, but the employment of the secondary structure to introduce function and dictate new morphologies is less explored. Short amphiphiles (also named peptide surfactants) demonstrate the formation of higher-order structures, but controlling the morphology is not clear and the employment of the secondary structure is absent.[28] Regardless, the impact of these amphiphilic peptides has demonstrated utility in stabilizing transmembrane proteins and enhancing their function. Producing helix-rich amphiphilic micelles by introducing longer heptad repeat units represents one avenue for engineering helix-rich sites, achieving a micellar conformation.[29] Similar transitions from α-helices to β-sheets in peptide amphiphiles have been noted before, but those sequences did not yield the bilayer assemblies that we target here.[30] As mentioned, β-sheet-rich assemblies dominate the field of peptide amphiphiles. This is simply because the intermolecular hydrogen bonding that stabilizes the assemblies is energetically favorable to van der Waals packing between aliphatic amino acids in small peptides. However, energetically favorable packing interactions in de novo-designed peptides have been engineered to yield highly ordered crystalline materials via helix−helix interfacing.[31] As such, our approach employs a popular helix motif, the leucine zipper, inspiring the simple, leucine-rich peptide amphiphile, K_3L_{12}.

Our approach highlights the ability to control the helix content with respect to pH, time, and temperature that yields a multitude of morphologies from a single peptide. From pH 1 to 7, we demonstrated the transition from α-helix to β-sheet-rich structures. At high pH values, we maintain a dominant α-helix assembly. The bilayer nature was achieved as evidenced by the AFM data at low pH values. However, upon heating, we observed the transition to β-sheet-rich, coiled disks where the leucine-rich faces pack together, as evidenced by AFM and small-angle X-ray scattering/wide-angle X-ray scattering (SAXS/WAXS) data. At high pH values, we observe α-helical-rich, large spherical assemblies that aggregate together. Upon heating, the assemblies transition into planklike bilayer structures in dense aggregates while maintaining a predominant α-helical character. All of these results highlight the importance of the secondary structure on nanoscale peptide assemblies. The bilayer assembly was our main target, as its dimensions resemble that of a lipid bilayer and imply that a functional bilayer assembly can ultimately be realized with some reengineering of the simple K_3L_{12} peptide. Future work will focus on exploring peptide designs that prevent the transition from α-helices to β-sheets and use engineered molecular interactions to tune the mechanical properties of the bilayer assemblies. Furthermore, by incorporating various cofactors (e.g., transition metals, metalloporphyrins, light-activated chromophores) in a well-defined, structured environment, we will be able to generate functional peptide membranes as simple analogs to transmembrane proteins in a lipid bilayer.

DOI: 10.1021/acs.langmuir.9b00424
Langmuir XXXX, XXX, XXX−XXX

■ ASSOCIATED CONTENT

Supporting Information

The Supporting Information is available free of charge on the ACS Publications website at DOI: 10.1021/acs.langmuir.9b00424.

Materials and methods; energy-minimized structures; reverse phase HPLC chromatogram; mass spectrometry; circular dichroism kinetics; Gaussian fits of FTIR data; dynamic light scattering; atomic force microscopy; height profiles; and SAXS/WAXS data (PDF)

■ AUTHOR INFORMATION

Corresponding Author

*E-mail: hfry@anl.gov.

ORCID

H. Christopher Fry: 0000-0001-8343-5189

Present Address

§Wellesley College, 106 Central Street, Wellesley, Massachusetts 02481, United States (H.M.C.).

Notes

The authors declare no competing financial interest.

■ ACKNOWLEDGMENTS

This material is based upon the work supported by Laboratory Directed Research and Development (LDRD), and the use of the Center for Nanoscale Materials was supported by the US Department of Energy, Office of Science, Office of Basic Energy Sciences, under contract no. DE-AC02-06CH11357. This research used resources of the Advanced Photon Source, a US Department of Energy (DOE) Office of Science User Facility operated for the DOE Office of Science by Argonne National Laboratory under contract no. DE-AC02-06CH11357 for small-angle X-ray scattering (SAXS) and wide-angle X-ray scattering (WAXS) measurements.

■ REFERENCES

(1) Hedin, L. E.; Illergard, K.; Elofsson, A. An Introduction to Membrane Proteins. *J. Proteome Res.* **2011**, *10*, 3324−3331.

(2) Engelman, D. M. Membranes are more mosaic than fluid. *Nature* **2005**, *438*, 578−580.

(3) Zhao, X. J. Design of self-assembling surfactant-like peptides and their applications. *Curr. Opin. Colloid Interface Sci.* **2009**, *14*, 340−348.

(4) Dalgicdir, C.; Globisch, C.; Peter, C.; Sayar, M. Tipping the Scale from Disorder to Alpha-helix: Folding of Amphiphilic Peptides in the Presence of Macroscopic and Molecular Interfaces. *PLoS Comput. Biol.* **2015**, *11*, No. e1004328.

(5) Hendricks, M. P.; Sato, K.; Palmer, L. C.; Stupp, S. I. Supramolecular Assembly of Peptide Amphiphiles. *Acc. Chem. Res.* **2017**, *50*, 2440−2448.

(6) Wu, Y. Y.; Collier, J. H. alpha-Helical coiled-coil peptide materials for biomedical applications. *Wiley Interdiscip. Rev.: Nanomed. Nanobiotechnol.* **2017**, *9*, No. e1424.

(7) Singh, N.; Kumar, M.; Miravet, J. F.; Ulijn, R. V.; Escuder, B. Peptide-Based Molecular Hydrogels as Supramolecular Protein Mimics. *Chem. - Eur. J.* **2017**, *23*, 981−993.

(8) Hamley, I. W. Small Bioactive Peptides for Biomaterials Design and Therapeutics. *Chem. Rev.* **2017**, *117*, 14015−14041.

(9) Zozulia, O.; Dolan, M. A.; Korendovych, I. V. Catalytic peptide assemblies. *Chem. Soc. Rev.* **2018**, *47*, 3621−3639.

(10) Woolfson, D. N. Building Fibrous Biomaterials From alpha-Helical and Collagen-Like Coiled-Coil Peptides. *Biopolymers* **2010**, *94*, 118−127.

(11) Burgess, N. C.; Sharp, T. H.; Thomas, F.; Wood, C. W.; Thomson, A. R.; Zaccai, N. R.; Brady, R. L.; Serpell, L. C.; Woolfson, D. N. Modular Design of Self-Assembling Peptide-Based Nanotubes. *J. Am. Chem. Soc.* **2015**, *137*, 10554−10562.

(12) Parmar, A. S.; James, J. K.; Grisham, D. R.; Pike, D. H.; Nanda, V. Dissecting Electrostatic Contributions to Folding and Self-Assembly Using Designed Multicomponent Peptide Systems. *J. Am. Chem. Soc.* **2016**, *138*, 4362−4367.

(13) Hernández, B.; Boukhalfa-Heniche, F. Z.; Seksek, O.; Coic, Y. M.; Ghomi, M. Secondary conformation of short lysine- and leucine-rich peptides assessed by optical spectroscopies: Effect of chain length, concentration, solvent, and time. *Biopolymers* **2006**, *81*, 8−19.

(14) Béven, L.; Castano, S.; Dufourcq, J.; Wieslander, A.; Wroblewski, H. The antibiotic activity of cationic linear amphipathic peptides: lessons from the action of leucine/lysine copolymers on bacteria of the class Mollicutes. *Eur. J. Biochem.* **2003**, *270*, 2207−2217.

(15) Bellomo, E. G.; Wyrsta, M. D.; Pakstis, L.; Pochan, D. J.; Deming, T. J. Stimuli-responsive polypeptide vesicles by conformation-specific assembly. *Nat. Mater.* **2004**, *3*, 244−248.

(16) Holowka, E. P.; Pochan, D. J.; Deming, T. J. Charged polypeptide vesicles with controllable diameter. *J. Am. Chem. Soc.* **2005**, *127*, 12423−12428.

(17) Sarkar, S.; Pandey, P. R.; Roy, S. Propensity of Self-Assembled Leucine-Lysine Diblock Copolymeric alpha-Helical Peptides To Remain in Parallel and Antiparallel Alignments in Water. *J. Phys. Chem. B* **2015**, *119*, 9520−9531.

(18) Fujiwara, K.; Toda, H.; Ikeguchi, M. Dependence of alpha-helical and beta-sheet amino acid propensities on the overall protein fold type. *BMC Struct. Biol.* **2012**, *12*, 18.

(19) Woolfson, D. N. The design of coiled-coil structures and assemblies. *Adv. Protein Chem.* **2005**, *70*, 79.

(20) Wimley, W. C.; Creamer, T. P.; White, S. H. Solvation energies of amino acid side chains and backbone in a family of host-guest pentapeptides. *Biochemistry* **1996**, *35*, 5109−5124.

(21) Wimley, W. C.; White, S. H. Experimentally determined hydrophobicity scale for proteins at membrane interfaces. *Nat. Struct. Biol.* **1996**, *3*, 842−848.

(22) Kong, J.; Yu, S. Fourier transform infrared spectroscopic analysis of protein secondary structures. *Acta Biochim. Biophys. Sin.* **2007**, *39*, 549−559.

(23) Park, K.; Perczel, A.; Fasman, G. D Differentiation between transmembrane helices and peripheral helices by the deconvolution of circular dichrisom spectra of membrane proteins. *Protein Sci.* **1992**, *1*, 1032−1049.

(24) Cerpa, R.; Cohen, F. E.; Kuntz, I. D. Conformational switching in designed peptides: The helix/sheet transition. *Folding Des.* **1996**, *1*, 91−101.

(25) Mutter, M.; Gassmann, R.; Buttkus, U.; Altmann, K. H. Switch peptides − pH induced alpha-helix to beta-sheet transitions of bis-amphiphilic oligopeptides. *Angew. Chem., Int. Ed.* **1991**, *30*, 1514−1516.

(26) Zhang, S. G.; Rich, A. Direct conversion of an oligopeptide from a beta-sheet to an alpha-helix: A model for amyloid formation. *Proc. Natl. Acad. Sci. USA* **1997**, *94*, 23−28.

(27) Qin, Z.; Buehler, M. J. Molecular Dynamics Simulation of the alpha-Helix to beta-Sheet Transition in Coiled Protein Filaments: Evidence for a Critical Filament Length Scale. *Phys. Rev. Lett.* **2010**, *104*, No. 198304.

(28) Koutsopoulos, S.; Kaiser, L.; Eriksson, H. M.; Zhang, S. G. Designer peptide surfactants stabilize diverse functional membrane proteins. *Chem. Soc. Rev.* **2012**, *41*, 1721−1728.

(29) Marullo, R.; Kastantin, M.; Drews, L. B.; Tirrell, M. Peptide contour length determines equilibrium secondary structure in protein-analogous micelles. *Biopolymers* **2013**, *99*, 573−581.

(30) Shimada, T.; Lee, S.; Bates, F. S.; Hotta, A.; Tirrell, M. Wormlike Micelle Formation in Peptide-Lipid Conjugates Driven by Secondary Structure Transformation of the Headgroups. *J. Phys. Chem. B* **2009**, *113*, 13711−13714.

DOI: 10.1021/acs.langmuir.9b00424
Langmuir XXXX, XXX, XXX−XXX

(31) Lanci, C. J.; MacDermaid, C. M.; Kang, S. G.; Acharya, R.; North, B.; Yang, X.; Qiu, X. J.; DeGrado, W. F.; Saven, J. G. Computational design of a protein crystal. *Proc. Natl. Acad. Sci. USA* **2012**, *109*, 7304−7309.

DOI: 10.1021/acs.langmuir.9b00424
Langmuir XXXX, XXX, XXX−XXX